ACS OMEGA

http://pubs.acs.org/journal/acsodf

Article

Applying Neuromorphic Computing Simulation in Band Gap Prediction and Chemical Reaction Classification

Baochen Li, Haibin Sun, Haonian Shu, and Xiaoxue Wang*

Cite This: *ACS Omega* 2022, 7, 168−175

Read Online

ACCESS | Metrics & More | Article Recommendations | Supporting Information

ABSTRACT: The rapidly developing artificial intelligence (AI) requires revolutionary computing architectures to break the energy efficiency bottleneck caused by the traditional von Neumann computing architecture. In addition, the emerging brain−machine interface also requires computational circuitry that can conduct large parallel computational tasks with low energy cost and good biocompatibility. Neuromorphic computing, a novel computational architecture emulating human brains, has drawn significant interest for the aforementioned applications due to its low energy cost, capability to parallelly process large-scale data, and biocompatibility. Most efforts in the domain of neuromorphic computing focus on addressing traditional AI problems, such as handwritten digit recognition and file classification. Here, we demonstrate for the first time that current neuromorphic computing techniques can be used to solve key machine learning questions in cheminformatics. We predict the band gaps of small-molecule organic semiconductors and classify chemical reaction types with a simulated neuromorphic circuitry. Our work can potentially guide the design and fabrication of elementary devices and circuitry for neuromorphic computing specialized for chemical purposes.

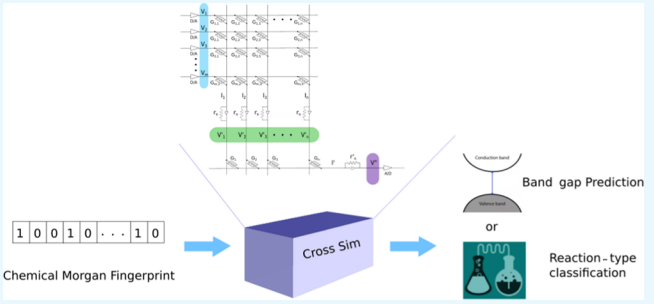

INTRODUCTION

The rapid development of artificial intelligence (AI) demands imminent response to the energy efficiency bottleneck brought by the conflict between the traditional von Neumann computational architecture and the rapidly evolving deep learning algorithms.[1] In the von Neumann architecture, the data movement between memory and processing units causes a large penalty of energy.[2] On the other hand, human brains consume orders of magnitude less energy but usually outperform modern computers in tasks such as image recognition and natural language analysis.[3] As an example of this energy efficiency gap, the training process of the first generation of AlphaGo, the famous deep learning model to play the strategy board game of Go, requires ∼5 × 10^5 W[4] as the peak power, while human brains work at only ∼20 W[5] but can easily defeat the early versions of AlphaGo. Neuromorphic computing can fill this energy gap by enabling the processing of big data within the memories to eliminate data movement, which can drastically reduce the energy consumption by ∼5 orders of magnitude.[6]

Recently, neuromorphic computing has been demonstrated with resistive memories or memristors based on various materials, including oxides,[7] phase change materials,[8] and polymers.[9] A memristor is a key device whose conductance can be tuned *via* programmed applied voltage pulses. In a matrix−vector multiplicator implemented *via* a crossbar circuit in neuromorphic computing (Figure 1a), the conductance of memristors acts as the weights of an abstract artificial neural network in machine learning algorithms (Figure 1b).[10] The input vectors are given in the form of voltages (in Figure 1b). As a result of Ohm's law and Kirchhoff's law, the output of the crossbar memory is naturally the results of vector−matrix multiplication operations. Therefore, by tuning and reading the conductance of memristors, training and inference of a neural network can be accomplished within memristors.

Traditionally, to complete vector−matrix multiplications in a conventional computational architecture, the process units need to fetch data from the dynamic random-access memory (DRAM) to obtain the weights and inputs, multiply inputs with the weights, and move data back to the DRAM, resulting in high energy consumption.[32] However, crossbar circuitry allows for in-memory computing and parallel reading. The memristors serve as the memory where the vector−matrix multiplication take place *in situ*. Parallel reading allows these operations to occur in a single step by mimicking the current summary in a parallel-connected circuit.[11] Parallel writing, which is also beneficial for energy usage, is used to update the weights;[11] weights (W_{ij}) are updated based on the outer

Received: August 10, 2021
Accepted: December 1, 2021
Published: December 17, 2021

https://doi.org/10.1021/acsomega.1c04287
ACS Omega 2022, 7, 168−175

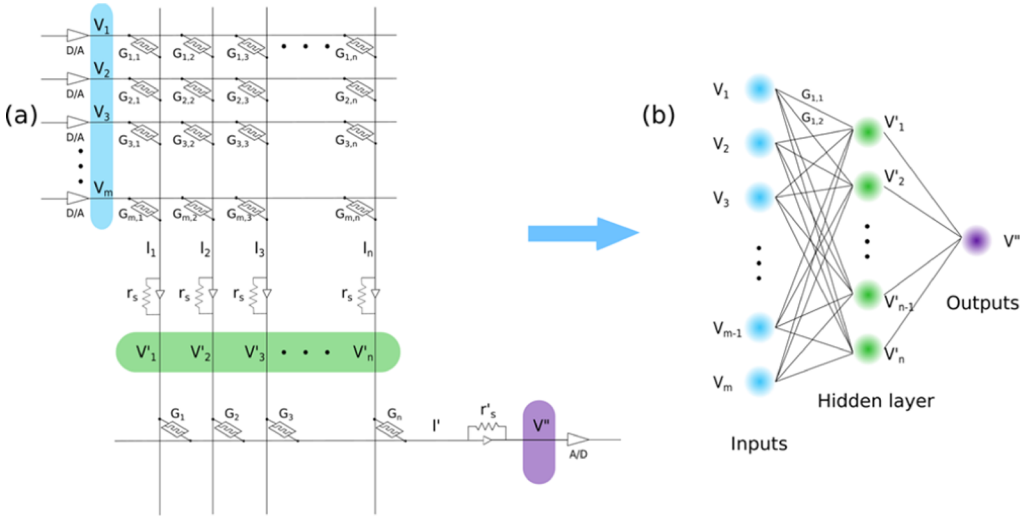

Figure 1. Schematic for the structure of (a) neuromorphic computing and its relationship with (b) neural networks.

product of the row (length of the voltage pulse x_i) and the column (height of the voltage pulse y_i), according to eq 1. It had been proven that for an $N \times N$ crossbar, analog resistive memory crossbars can be $O(N)$ more energy-efficient than a conventional digital memory-based architecture.[11]

$$W' = W + x \otimes y$$
or
$$W'_{ij} = W_{ij} + x_i y_j \quad (1)$$

To estimate the performance of a memristor in a neuromorphic computing circuit quickly without fabricating such a circuit, neuromorphic computing simulation software packages, such as CrossSim[26] and NeuroSim,[27] have attracted much attention. Fuller *et al.*[7−9] used CrossSim to perform classification in backpropagation simulations on handwritten digits and file classification on a Sandia data set. Yu *et al.*[12,13] added hybrid precision synapse and advanced learning algorithms in NeuroSim to increase the Modified National Institute of Standards and Technology (MNIST)[28] handwritten recognition accuracy. The accuracy and energy consumption for the training of MNIST images with different emerging nonvolatile memories are also compared using NeuroSim in 2018.[2] Additionally, Chen *et al.* used MATLAB to simulate the classification performance of their memristive synapse for neuromorphic computing.[14] Wang *et al.*[15] used SPICE[29] to simulate an in-memory computing system based on a resistive random-access memory crossbar circuit, which can perform parallel and general computing tasks, and indicated that this architecture could handle with data-intensive problems. Hu *et al.*[16] developed a dot product engine with transistor−memristor arrays and combined it with MATLAB to formulate a single-layer neural network for MNIST handwritten classification, achieving 89.9% recognition accuracy.

At the same time, machine learning has found wide application in cheminformatics, for example, generating molecules with desired properties,[17,30,31] predicting pharmaceutical properties for drug-like compounds,[18] and so forth. Similar to other AI applications, the exciting applications of machine learning in cheminformatics calls for energy-efficient computational hardware. The decent feature of the neuromorphic architecture is suitable for machine learning tasks in cheminformatics. However, few studies have been conducted for this application. Here, we introduce CrossSim into chemistry-related machine learning objectives. As an example of regression tasks, we used CrossSim to predict the band gap of small-molecule organic semiconductors; as an example of classification tasks, we used CrossSim to classify chemical reactions. We conducted experiments on the band gap prediction with different materials' lookup tables. In CrossSim, the weight update is based on lookup tables that are acquired from experiments. The lookup tables provide the information of the probability distribution of conductance change at a given conductance by the applied voltage pulse.[26] After comparing three materials including a lithium-ion synaptic transistor,[8] tantalum oxide (TaOx)-based resistive memories,[7] and an electrochemical neuromorphic organic device,[9] we found that the lithium-ion synaptic transistor has the lowest loss, while tantalum oxide-based resistive memories exhibit a fluctuation with increasing training epochs in the regression task to predict the band gaps for organic semiconductors. To reveal the reason why the fluctuation exists in TaOx-based memristors, we trained two sequential crossbar circuits with different lookup tables (i.e., circuits based on different materials). We found that the performance of TaOx memristors depends on the dimension of the crossbar circuit, and they tend to underperform in relatively small crossbar arrays (50×1). This phenomenon may be due to the write noise intrinsic to TaOx memristors.[7] To demonstrate the ability of neuromorphic computing for classification applications, another network was trained to classify the chemical reaction types from a reaction database, USPTO-50k.[24] We obtained consistent results between the CrossSim simulation and the widely used deep learning application programming interface (API) Keras. Due to the imbalance of the data set, undersampling[19] was applied to data-abundant reaction types. Compared to previous outcomes, CrossSim training after undersampling showed higher classification precision and less false positive cases. Our work demonstrates that neuromorphic computing techniques can be used in cheminformatic problems well and further discusses the material dependency on the training performance. Our work can potentially be used to guide the design and

https://doi.org/10.1021/acsomega.1c04287
ACS Omega 2022, 7, 168−175

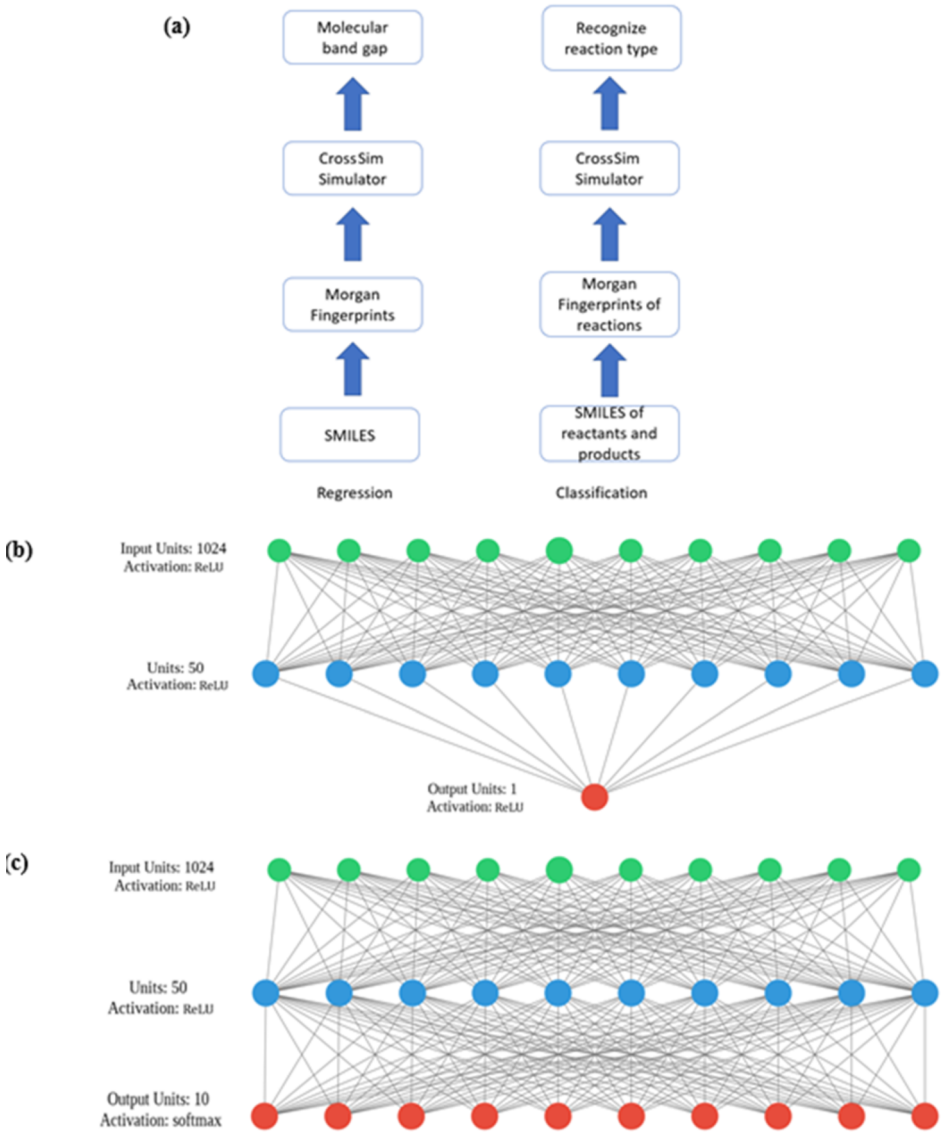

Figure 2. (a) Schematic for applying a CrossSim simulator to solve simple chemical neural network problems; (b) architecture of the neural network for band gap prediction; and (c) architecture of the neural network for reaction type classification. ReLU: rectified linear unit.

fabrication of devices and circuitry for neuromorphic computing specialized for chemical purposes.

METHODS

Molecular Band Gap Prediction. Band gap is an important electronic and optical property for organic semiconductors. However, calculating the band gap from the density functional theory (DFT) requires many resources. We can leverage machine learning to predict the band gaps at a much lower cost.[11] The data source used for the molecular band gap prediction was obtained from the literature, calculated by the DFT.[20] The database is composed of a total number of 111,725 molecules. These molecules were given as xyz files and transformed to the canonical simplified molecular-input line-entry system (SMILES) molecular representation.[21] Then, the SMILES strings were converted into Morgan Fingerprints[22] with digits of 1024 and a radius of 2 by RDKit.[23] The Morgan fingerprints are the input for memristors. The whole data set was split into a training set and a test set in a ratio of 9:1. Molecular fingerprints were treated as the input signal for the neuromorphic simulation in CrossSim. To ensure that the initialization of the simulation is the same, we used identical seeds to set up the training processes. The flowchart of this regression task is shown in the first panel of Figure 2a. The architecture of the neural network is shown in Figure 2b. The output layer generates a band gap value for each input molecular fingerprint. The loss function between the predicted band gap and actual band gap is the mean squared error (MSE) and was optimized by back-propagation. Similar to the weight update in neural network training, conductance at each intersection in Figure 1 was alternated through the applied voltage to move the predicted values close to actual band gap values. The conductance update was accomplished based on a conductance change lookup table. This lookup table was generated from experimental measurements. The numerical weights in the network layer are mapped directly onto the experimental device conductance states. The statistics of the conductance change is included in the lookup table. For the back-propagation, the weights were programmed by the lookup table. To update a weight, the initial state of the device, G_0, is

https://doi.org/10.1021/acsomega.1c04287
ACS Omega 2022, 7, 168−175

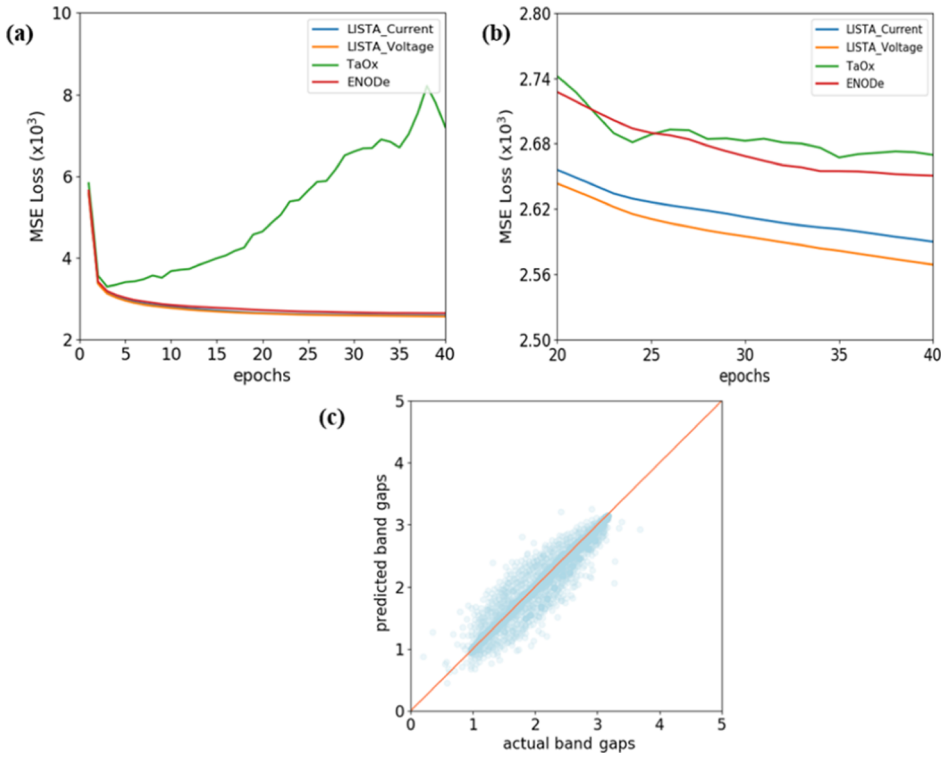

Figure 3. (a) Average loss for different lookup tables with the lookup table possibility distribution range [0.25, 0.75] for training; (b) average loss for different lookup tables with the lookup table possibility distribution range [0.1, 0.9] for training; (c) actual *vs* predicted result for the LISTA_Current simulation with the lookup table range from 0.1 to 0.9 at epoch 40 for the test set.

determined and next, the state is updated by the average change ΔG; ΔG is scaled based on the updated size calculated by the backpropagation.[9] Therefore, the behavior of each material can be estimated when they are used in a neuromorphic circuit if the relationship between the conductance and applied voltage is measured. In this work, the following four lookup tables were obtained from the literature: current-controlled pulses measurement for the lithium-ion synaptic transistor (LISTA_Current);[8] voltage-controlled pulses measurement for the lithium-ion synaptic transistor (LISTA_Voltage);[8] tantalum oxide-based resistive memories (TaOx);[7] and an electrochemical neuromorphic organic device (ENODe).[9] LISTA is an all-solid-state non-volatile redox transistor with a resistance switching mechanism based upon the intercalation of Li-ion dopants into a channel of $Li_{1-x}CoO_2$.[8] TaOx switches the resistance based on an oxygen vacancy exchange between the TaOx layer and the Ta layer upon the application of an external electric signal.[7] The device architecture for ENODe is a poly(ethylenimine) (PEI)/poly(3,4-ethylenedioxythiophene):polystyrene sulfonate (PEDOT:PSS) film serving as the postsynaptic electrode, interfaced with a PEDOT:PSS presynaptic electrode *via* an electrolyte. Upon applying a potential to the PEDOT:PSS electrode, cations are transported to the PEI/PEDOT:PSS layer and resulting holes are removed from PEDOT in the postsynaptic electrode, thereby reducing its conductivity.[9] According to the references, the device area for TaOx is 0.9 × 0.9 μm^2 and the area for ENODe is 0.3 × 0.3 μm^2. These four types of materials were applied and tested in this band gap prediction task to identify the strength and weakness for the specific purpose.

Chemical Reaction Classification. The database for the chemical reaction classification was USPTO-50k.[24] USPTO contained chemical reactions from US patents from 1976 to 2016. Information about the reaction types, product SMILES, and reactant SMILES was included in the database. Reactions in USPTO-50k were single-step reactions and grouped into 10 reaction classes, Rx_1 to Rx_10, referring to heteroatom alkylation and arylation, acylation and related processes, C−C bond formation, heterocycle formation, protections, deprotections, reductions, oxidations, functional group interconversion, and functional group addition,[24] respectively. The entire database was split into a training set and a test set in a ratio of 9:1 with the same reaction type ratios. We used Morgan fingerprints of reactions, the difference between the fingerprint of the product and reactants, as inputs for CrossSim. The dimensions of the network were set to be 1024, 50, and 10 nodes for the input layer, hidden layer, and output layer, respectively, as shown in Figure 2c. The goal was to identify the class of a reaction based on its reactants and product. The backpropagation algorithm together with the gradient descent was applied to update the weights during the training process. Additionally, the lookup table used to adjust the conductance in CrossSim was LISTA_Current. Later, the classification result from the CrossSim simulation was compared to that from Keras,[25] an API for implementing neural networks, with an identical network architecture and algorithm.

RESULTS AND DISCUSSION

Prediction for the Band Gap of Small Organic Molecules. Prediction of the band gap of a small organic molecule was first performed using the four lookup tables with the conductance change probability distribution in the range [0.25, 0.75], which was recommended by the manual of CrossSim software.[26] As shown in Figure 3a, the average losses of LISTA_Current (current-controlled pulse measurement for

https://doi.org/10.1021/acsomega.1c04287
ACS Omega 2022, 7, 168−175

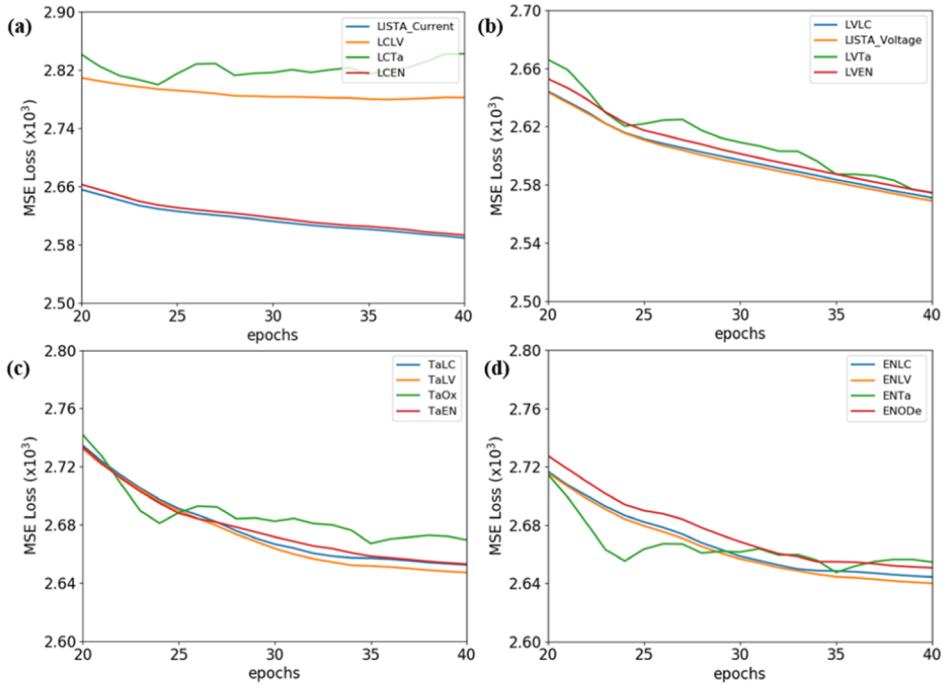

Figure 4. Using different materials to simulate the band gap prediction for training. (a) LISTA_Current: both crossbars using LISTA_Current; LCLV: first crossbar using LISTA_Current and second crossbar using LISTA_Voltage; LCTa: first crossbar using LISTA_Current and second crossbar using TaOx; and LCEN: first crossbar using LISTA_Current and second crossbar using ENODe; (b) LISTA_Voltage: both crossbars using LISTA_Voltage; LVLC: first crossbar using LISTA_Voltage and second crossbar using LISTA_Current; LVTa: first crossbar using LISTA_Voltage and second crossbar using TaOx; and LVEN: first crossbar using LISTA_Voltage and second crossbar using ENODe; (c) TaOx: both crossbars using TaOx; TaLC: first crossbar using TaOx and second crossbar using LISTA_Current; TaLV: first crossbar using TaOx and second crossbar using LISTA_Voltage; and TaEN: first crossbar using TaOx and second crossbar using ENODe; and (d) ENODe: both crossbars using ENODe; ENLC: first crossbar using ENODe and second crossbar using LISTA_Current; ENLV: first crossbar using ENODe and second crossbar using LISTA_Voltage; and ENTa: first crossbar using ENODe and second crossbar using TaOx.

the $Li_{1-x}CoO_2$-based lithium-ion synaptic transistor),[8] LISTA_Voltage (voltage-controlled pulse measurement for the $Li_{1-x}CoO_2$-based lithium-ion synaptic transistor),[8] and ENODe (PEI/PEDOT:PSS)[9] converged normally, but the loss of TaOx[7] did not converge after five or six epochs. The learning rate was explored for better performance, but it did not change the result of TaOx prediction, as shown in Figure S1. Ideal results were gained by enlarging the possibility distribution range to [0.1, 0.9]. The performances of the available materials are compared in Figure 3b. Generally, LISTA_Current and LISTA_Voltage had a smaller average loss than TaOx and ENODe, which indicates that the material for LISTA ($Li_{1-x}CoO_2$) may be the favorite material to fabricate a physical device to make predictions on molecular band gaps. Figure 3c shows the comparison between the actual band gaps and predictions for the test set using the LISTA_Current lookup table, where the coefficient of determination is 0.96. This prediction result was comparable to the result obtained from the regression with TensorFlow Keras, where the coefficient of determination is 0.98. In addition, the TaOx prediction result in Figure 3b fluctuated with increasing epochs. To find out the reason of fluctuation, research on the simulation of different materials for the two crossbars was conducted. The results are discussed in the following paragraph.

Crossbar networks with dimensions of (1024, 50) and (50, 1) were simulated with different lookup tables in CrossSim, as shown in Figure 2b. The simulation results are shown in Figure 4. Fluctuations were observed in each figure when the TaOx lookup table was utilized for the (50, 1) crossbar network. In Figure 4c, the network with the dimension of (1024, 50) was completely simulated with the TaOx lookup table, and the network with a dimension of (50, 1) was simulated with other materials. It was demonstrated that the fluctuation in the TaOx simulation was caused by the (50, 1) network. According to the application of TaOx-based resistive memories on handwritten digit recognition,[7] we think this perturbation on a small-dimension crossbar network is caused by the intrinsic write noise of this material.[33] If the dimension of the crossbar network is small, the write noise will exhibit a large impact on the crossbar performance. However, the influence of this write noise can be neglected when TaOx is applied in large-dimension crossbar networks. Therefore, TaOx can capture features of large-dimension networks but lacks the ability to fit the results with small-dimension crossbar networks.

In addition, a two-hidden-layer model for the band gap prediction task was implemented. Dimension of the model was set to be (1024, 50, 50, 1). Also, the three crossbars were all simulated with the LISTA_Current lookup table. The training result is shown in Figure S3. It took more epochs, about 160 epochs, for the MSE loss to reach a steady state, and the loss was around 0.00282, which was close to the result we obtained from the one-hidden-layer model whose loss was 0.00285. After that, the test set was tested on the two-hidden-layer model, and a coefficient of determination of around 0.98 was obtained. As mentioned previously, the coefficient of determination for the one-hidden-layer model is 0.96. Upon comparing the results from these two models, we believe that the one-hidden-layer model was sufficient for the band gap

https://doi.org/10.1021/acsomega.1c04287
ACS Omega 2022, 7, 168−175

Table 1. Classification Result Comparison between CrossSim and Keras

		CrossSim		Keras		
		precision	true positive + false positive	precision	true positive + false positive	number of reactions in the test set
RX_1	heteroatom alkylation and arylation	0.756	1835	0.763	1935	1500
RX_2	acylation and related processes	0.721	1521	0.737	1464	1190
RX_3	C−C bond formation	0.698	357	0.717	346	550
RX_4	heterocycle formation	0.663	70	0.789	61	90
RX_5	protection	0.594	18	0.441	23	65
RX_6	deprotection	0.647	763	0.676	772	825
RX_7	reduction	0.712	276	0.701	238	450
RX_8	oxidation	0.574	48	0.556	57	80
RX_9	functional group interconversion	0.473	110	0.499	103	160
RX_10	functional group addition	0.5	2	1	1	25

prediction task. Moreover, the training result for a three-hidden-layer model is provided in the Supporting Information.

Classifying Chemical Reactions. In Table 1, classification results obtained using CrossSim (based on LISTA_Current lookup table) and Keras are listed. The precision is defined as the number of correctly classified reactions (true positive) divided by the total number of reactions being classified as belonging to a specific reaction type (true positive + false positive). Higher precision was obtained for reaction types with larger data amount. Table S1 shows the recall of both CrossSim and Keras classification models. Recall is defined as the number of true positive cases divided by the summation of true positive and false negative cases. As shown in Table 1 and S1, no obvious difference in the performance could be discovered between the two models. Therefore, we believed that the classification task accomplished by CrossSim was comparable to that completed by Keras. Because the USPTO-50k database is not balanced between reaction types, we adopted the undersampling strategy[19] on the majority of classes in the training set to seek for a better classification performance. As a result of undersampling, Rx_1 and Rx_2 were diminished by 20% in the training set; Rx_3 and Rx_6 were reduced by 10%. The classification for CrossSim with an undersampling strategy is shown in Tables 2 and S2. The numbers of false positive cases for data-abundant reaction types are decreased. Therefore, the precision of classification is increased with the application of the undersampling strategy.

Table 2. Classification Result for CrossSim with Undersampling

	CrossSim with undersampling	
	precision	true positive + false positive
RX_1	0.902	1536
RX_2	0.805	1152
RX_3	0.704	597
RX_4	0.788	80
RX_5	0.540	87
RX_6	0.655	875
RX_7	0.903	380
RX_8	0.514	107
RX_9	0.421	183
RX_10	1	3

CONCLUSIONS

Neuromorphic computing simulation is accomplished within a crossbar simulator CrossSim. The energy consumption can be dramatically reduced if the widely used von Neumann architecture can be substituted by neuromorphic computing devices. Unlike other studies on machine learning applications in cheminformatics, we used the CrossSim simulator to solve chemical problems, namely, organic molecular band gap prediction and chemical reaction type classification. In the task of predicting the band gaps of small-molecule organic semiconductors, different lookup tables of different memristors are applied in CrossSim at the conductance changing possibility distribution range of [0.1, 0.9] to overcome the divergence when TaOx is applied as the conductance update policy. Among these memristors, LISTA exhibits the smallest loss. This suggests that LISTA will be the best choice for fabricating a neuromorphic device to predict small organic molecular band gaps. According to the comparison of different memristors in two crossbar networks, we obtain the conclusion that TaOx may not be appropriate to be used as a conductance update policy for networks with relatively small dimensions. This phenomenon may be due to the relatively high write noise of TaOx-based memristors. Regarding the classification problem, the accuracy and prediction amount attained by CrossSim are close to those by Keras, and better performance can be achieved by undersampling the reaction types with more abundant data. Our work can potentially inspire the following studies that focus on generating lookup tables for novel neuromorphic materials in CrossSim and applying them in other chemical problems.

ASSOCIATED CONTENT

Supporting Information

The Supporting Information is available free of charge at https://pubs.acs.org/doi/10.1021/acsomega.1c04287.

Learning rate impact on the tantalum oxide lookup table for band gap prediction; training result for band gap prediction using the one-hidden-layer model with 100 epochs; training result for band gap prediction using the two-layer model; training result for band gap prediction using the three-layer model; comparison of CrossSim and Keras: recall and true positive cases for reaction-type classification; and recall and true positive cases for CrossSim with undersampling (PDF)

https://doi.org/10.1021/acsomega.1c04287
ACS Omega 2022, 7, 168−175

AUTHOR INFORMATION

Corresponding Author

Xiaoxue Wang − *Department of Chemical and Biomolecular Engineering, The Ohio State University, Columbus, Ohio 43210, United States; The Ohio State University Sustainability Institute, Columbus, Ohio 43210, United States;* orcid.org/0000-0002-7231-9841; Email: wang.12262@osu.edu

Authors

Baochen Li − *Department of Chemical and Biomolecular Engineering, The Ohio State University, Columbus, Ohio 43210, United States*

Haibin Sun − *Department of Chemical and Biomolecular Engineering, The Ohio State University, Columbus, Ohio 43210, United States*

Haonian Shu − *Department of Chemical and Biomolecular Engineering, The Ohio State University, Columbus, Ohio 43210, United States*

Complete contact information is available at: https://pubs.acs.org/10.1021/acsomega.1c04287

Notes

The authors declare no competing financial interest.

ACKNOWLEDGMENTS

The authors would like to acknowledge the financial support from the Ohio State University. This work was partially supported by OSU President's Research Excellence (PRE) Accelerator Grant program. In addition, this work was supported in part by The Ohio State University Materials Research Seed Grant Program, funded by the Center for Emergent Materials, an NSF-MRSEC, grant DMR-2011876, the Center for Exploration of Novel Complex Materials, and the Institute for Materials Research.

REFERENCES

(1) Sebastian, A.; Le Gallo, M.; Khaddam-Aljameh, R.; Eleftheriou, E. Memory devices and applications for in-memory computing. *Nat. Nanotechnol.* **2020**, *15*, 529−544.

(2) Yu, S. Neuro-inspired computing with emerging nonvolatile memorys. *Proc. IEEE* **2018**, *106*, 260−285.

(3) Merkel, C.; Kudithipudi, D. Neuromemristive Systems: A Circuit Design Perspective. In *Advances in Neuromorphic Hardware Exploiting Emerging Nanoscale Devices*; Suri, M., Eds.; Springer India: New Delhi, 2017; pp 45−64.

(4) Wang, Z.; Li, C.; Song, W.; Rao, M.; Belkin, D.; Li, Y.; Yan, P.; Jiang, H.; Lin, P.; Hu, M.; Strachan, J. P.; Ge, N.; Barnell, M.; Wu, Q.; Barto, A. G.; Qiu, Q.; Williams, R. S.; Xia, Q.; Yang, J. J. Reinforcement learning with analogue memristor arrays. *Nat. Electron.* **2019**, *2*, 115−124.

(5) Ling, H.; Koutsouras, D. A.; Kazemzadeh, S.; van de Burgt, Y.; Yan, F.; Gkoupidenis, P. Electrolyte-gated transistors for synaptic electronics, neuromorphic computing, and adaptable biointerfacing. *Appl. Phys. Rev.* **2020**, *7*, 011307.

(6) Taha, T. M.; Hasan, R.; Yakopcic, C.; McLean, M. R. Exploring the Design Space of Specialized Multicore Neural Processors. *Proceedings of the International Joint Conference on Neural Networks*, 2013.

(7) Agarwal, S.; Jacobs Gedrim, R. B.; Hsia, A. H.; Hughart, D. R.; Fuller, E. J.; Talin, A. A.; James, C. D.; Plimpton, S. J.; Marinella, M. J. Achieving Ideal Accuracies in Analog Neuromorphic Computing Using Periodic Carry. *Digest of Technical Papers-Symposium on VLSI Technology*, 2017.

(8) Fuller, E. J.; El Gabaly, F.; Léonard, F.; Agarwal, S.; Plimpton, S. J.; Jacobs-Gedrim, R. B.; James, C. D.; Marinella, M. J.; Talin, A. A. Li-Ion Synaptic Transistor for Low Power Analog Computing. *Adv. Mater.* **2017**, *29*, 1604310.

(9) Van De Burgt, Y.; Lubberman, E.; Fuller, E. J.; Keene, S. T.; Faria, G. C.; Agarwal, S.; Marinella, M. J.; Alec Talin, A.; Salleo, A. A Non-Volatile Organic Electrochemical Device as a Low-Voltage Artificial Synapse for Neuromorphic Computing. *Nat. Mater.* **2017**, *16*, 414−418.

(10) Hu, M.; Li, H.; Chen, Y.; Wu, Q.; Rose, G. S.; Linderman, R. W. Memristor Crossbar-Based Neuromorphic Computing System: A Case Study. *IEEE Trans. Neural Networks Learn. Syst.* **2014**, *25*, 1864−1878.

(11) Agarwal, S.; Quach, T. T.; Parekh, O.; Hsia, A. H.; DeBenedictis, E. P.; James, C. D.; Marinella, M. J.; Aimone, J. B. Energy Scaling Advantages of Resistive Memory Crossbar Based Computation and Its Application to Sparse Coding. *Front. Neurosci.* **2015**, *9*, 484.

(12) Luo, Y.; Peng, X.; Yu, S. MLP+NeuroSiMv3.0: Improving on-Chip Learning Performance with Device to Algorithm Optimizations. *ACM International Conference Proceeding Series*, 2019.

(13) Chen, P. Y.; Yu, S. Reliability Perspective of Resistive Synaptic Devices on the Neuromorphic System Performance. *2018 IEEE International Reliability Physics Symposium (IRPS)*, 2018; pp 41−44.

(14) Chen, J.; Lin, C.-Y.; Li, Y.; Qin, C.; Lu, K.; Wang, J.-M.; Chen, C.-K.; He, Y.-H.; Chang, T.-C.; Sze, S. M.; Miao, X.-S. LiSiOX-Based Analog Memristive Synapse for Neuromorphic Computing. *IEEE Electron Device Lett.* **2019**, *40*, 542−545.

(15) Wang, X.; Zidan, M. A.; Lu, W. D.; Lu, W. D. A Crossbar-Based In-Memory Computing Architecture. *IEEE Trans. Circuits Syst.* **2020**, *67*, 4224−4232.

(16) Hu, M.; Graves, C. E.; Li, C.; Li, Y.; Ge, N.; Montgomery, E.; Davila, N.; Jiang, H.; Williams, R. S.; Yang, J. J.; Xia, Q.; Strachan, J. P. Memristor-Based Analog Computation and Neural Network Classification with a Dot Product Engine. *Adv. Mater.* **2018**, *30*, 1705914.

(17) Yang, K.; Swanson, K.; Jin, W.; Coley, C.; Eiden, P.; Gao, H.; Guzman-Perez, A.; Hopper, T.; Kelley, B.; Mathea, M.; Palmer, A.; Settels, V.; Jaakkola, T.; Jensen, K.; Barzilay, R. Analyzing Learned Molecular Representations for Property Prediction. *J. Chem. Inf. Model.* **2019**, *59*, 3370−3388.

(18) Krishnan, S. R.; Bung, N.; Bulusu, G.; Roy, A. Accelerating de Novo Drug Design against Novel Proteins Using Deep Learning. *J. Chem. Inf. Model.* **2021**, *61*, 621−630.

(19) Fernández, A.; García, S.; Herrera, F.; Chawla, N. V. SMOTE for Learning from Imbalanced Data: Progress and Challenges, Marking the 15-Year Anniversary. *J. Artif. Intell. Res.* **2018**, *61*, 863−905.

(20) Pereira, F.; Xiao, K.; Latino, D. A. R. S.; Wu, C.; Zhang, Q.; Aires-De-Sousa, J. Machine Learning Methods to Predict Density Functional Theory B3LYP Energies of HOMO and LUMO Orbitals. *J. Chem. Inf. Model.* **2017**, *57*, 11−21.

(21) Weininger, D.; Weininger, A.; Weininger, J. L. SMILES. 2. Algorithm for generation of unique SMILES notation. *J. Chem. Inf. Model.* **1989**, *29*, 97−101.

(22) Morgan, H. L. The Generation of a Unique Machine Description for Chemical Structures-A Technique Developed at Chemical Abstracts Service. *J. Chem. Doc.* **1965**, *5*, 107−113.

(23) RDKit: Open-source cheminformatics. https://www.rdkit.org.

(24) Schneider, N.; Stiefl, N.; Landrum, G. A. What's What: The (Nearly) Definitive Guide to Reaction Role Assignment. *J. Chem. Inf. Model.* **2016**, *56*, 2336−2346.

(25) Chollet, F.; et al. *Keras*, 2015; Available at: https://github.com/fchollet/keras.

(26) Agarwal, S.; Plimpton, S. J.; Schiek, R. L.; Richter, I.; Hsia, A. H.; Hughart, D. R.; Jacobs-Gedrim, R. B.; James, C. D.; Marinella, M. J.; Sim, R. *CrossSim: Crossbar Simulator*, Version 0.2, 2017; 0−19.

(27) Chen, P. Y.; Peng, X.; Yu, S. NeuroSim + : An Integrated Device - to - Algorithm Framework for Benchmarking Synaptic

https://doi.org/10.1021/acsomega.1c04287
ACS Omega 2022, 7, 168−175

Devices and Array Architectures. *IEEE International Electron Devices Meeting*, 2017; pp 135−138.
(28) LeCun, Y.; Cortes, C.; Burges, C. THE MNIST DATABASE of handwritten digits. http://yann.lecun.com/exdb/mnist/.
(29) Nagel, L. W.; Pederson, D. O. *SPICE (Simulation Program with Integrated Circuit Emphasis), Memorandum No. ERL-M382*; University of California: Berkeley, April 1973.
(30) Li, J.; Lim, K.; Yang, H.; Ren, Z.; Raghavan, S.; Chen, P.-Y.; Buonassisi, T.; Wang, X. AI Applications through the Whole Life Cycle of Material Discovery. *Matter* **2020**, *3*, 393−432.
(31) Chen, H.; Engkvist, O.; Wang, Y.; Olivecrona, M.; Blaschke, T. The Rise of Deep Learning in Drug Discovery. *Drug Discovery Today* **2018**, *23*, 1241−1250.
(32) Mutlu, O.; Ghose, S.; Gómez-Luna, J.; Ausavarungnirun, R. Processing data where it makes sense: Enabling in-memory computation. *Microprocess. Microsyst.* **2019**, *67*, 28−41.
(33) Agarwal, S.; Plimpton, S. J.; Hughart, D. R.; Hsia, A. H.; Richter, I.; Cox, J. A.; James, C. D.; Marinella, M. J. Resistive Memory Device Requirements for a Neural Algorithm Accelerator. *International Joint Conference on Neural Networks*, 2016; pp 929−938.

https://doi.org/10.1021/acsomega.1c04287
ACS Omega 2022, 7, 168−175